Porcupine-inspired microneedles coupled with an adhesive back patching as dressing for accelerating diabetic wound healing

Tianqi Liu [a,b], Guohua Jiang [a,b,*], Yanfang Sun [c,*], Wenjing Zhang [a,b], Rui Wang [a,b], Khaydar E. Yunusov [d], Uladzislau E. Aharodnikau [e], Sergey O. Solomevich [e], Lei Nie [f,g], Amin Shavandi [f]

[a] *School of Materials Science and Engineering, Zhejiang Sci-Tech University, Hangzhou, 310018, China*

[b] *International Scientific and Technological Cooperation Base of Intelligent Biomaterials and Functional Fibers, Hangzhou, 310018, China*

[c] *College of Life Sciences and Medicine, Zhejiang Sci-Tech University, Hangzhou, Zhejiang, 310018, China*

[d] *Institute of Polymer Chemistry and Physics, Uzbekistan Academy of Sciences, Tashkent, 100128, Uzbekistan*

[e] *Research Institute for Physical Chemical Problems of the Belarusian State University, Minsk, 220030, Belarus*

[f] *BioMatter unit-École polytechnique de Bruxelles, Université Libre de Bruxelles, Brussels, Belgium*

[g] *College of Life Sciences, Xinyang Normal University, Xinyang 464000, China*

E-mail, ghjiang_cn@zstu.edu.cn (G. Jiang)

katherineyfs@zzstu.edu.cn (Y. Sun)

Abstract: Diabetes chronic wound is a serve and frequently occurring medical issues in patients with diabetes that often lead to more serious complications. Microneedle (MN) patches can be used for wound healing since they are able to efficiently pierce the epidermis and deliver drugs into wound tissue. However, regular MN patches cannot provide adequate skin adhesion to prevent them from shedding on the wound area. Herein, inspired by natural hangnail microstructure of porcupine quills, we designed a porcupine quill-like multilayer MN patch with an adhesive back patching for tissue adhesion and diabetic wound healing. Sodium hyaluronate-modified CaO_2 nanoparticles (CaO_2-HA NPs) and metformin (hypoglycemic agent) were loaded into the polycaprolactone tips of microneedles, endowing them with exceptional antibacterial ability and hypoglycemic effect. The flexible and adhesive back patching was formed by polyacrylamide (PAM) composite hydrogel which ensure the MN patches could not been peeled off from the application sites and reduce bacterial infection. The bio-inspired multilayer structure MN patches exhibit excellent mechanical and antibacterial properties, which have a potential multifunctional dressing platform for promoting wound healing.

Keyword: Microneedle patches; transdermal delivery; wound healing; blood glucose levels; tissue Regeneration; skin adhesion

Graphic Abstract

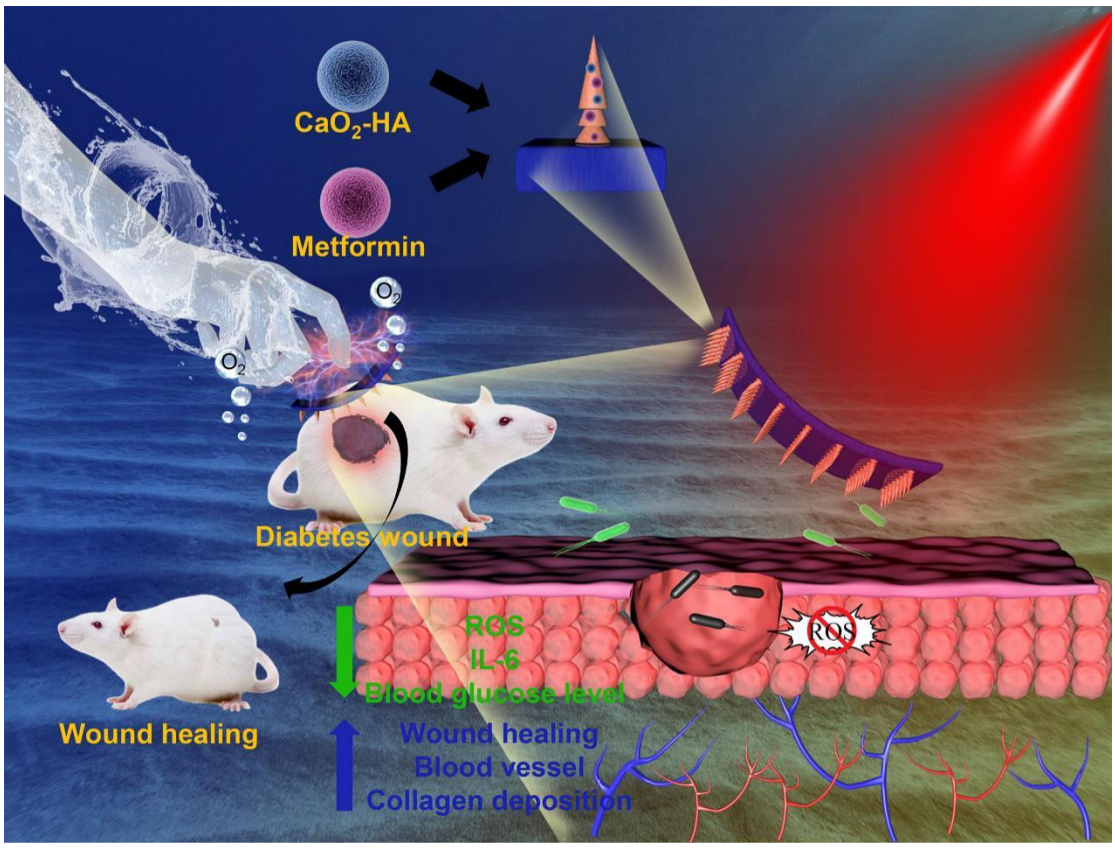

1. Introduction

Wound healing has always been a major challenge for diabetic patients, which leads to mortality and morbidity due to several pathological complications such as severe sepsis, systemic inflammatory responses and amputation of limbs [1]. There is an impairment in neovascularisation, angiogenesis and failure in keratinocyte, matrix metalloproteineases (MMPs) and fibroblast functions with increased production of reactive oxygen species (ROS) and advanced glycation end products (AGEs) for diabetic patients, ultimately leading to delayed wound healing [2,3]. Consequently, infections and ulcers are more likely to occur in diabetic patients, which eventually result in gangrene. Developing wound healing dressing that can provide a protective barrier and promote healing is highly desirable for management of chronic diabetic wounds.

Over the past few decades, great efforts have been devoted to development of the suitable wound healing dressings for accelerating the wound healing process, such as powder [4], foams [5], hydrocolloids [6], sponges [7], hydrogel [8], films [9], microneedle (MN) patches [10] and so on. Among them, MN patches has been proposed as a versatile technique and has obtained remarkable achievements in drug delivery [11], biosensors [12] and tissue healing [13] due to the advantages of painless and minimally invasive. Because of their good structural and excellent loading capacity compare with general drug delivery carriers, MN patches can effectively realize the loading of bioactive substances such as macromolecular drugs [14], cells [15], vaccines [16] and so on. And different strategies are currently being applied in diabetes wound healing by MN

patches, 1) control the blood glucose and take care of wounds [17], 2) antibacterial effect by loading traditional Chinese herb [18] or nanoparticles [19] and photothermal therapy (PTT) [20], 3) scavenging reactive oxygen species (ROS) [21]. However, general MN patches could not adhere well to the skin tissue and would fall off from the skin easily due to its elasticity and mobility [22]. The MN patches designed for a continuous drug delivery process will be considered ineffective if they are detached from the application sites [23,24]. In addition, there is a risk of bacterial infection from MN patches piercing the skin [25]. In order to overcome these objectives, new MN patches should provide 1) enough attachment time to efficient delivery of the drugs, 2) improved skin adhesion to prevent them from shedding during the movement, and 3) excellent antibacterial ability to avoid bacterial infection [26-28].

Over the past decade, numerous studies have focused on improving the adhesion properties of MN patches. Chemical adhesives are commonly used due to their low cost and high strength, but they have inflammatory or toxic side effects [29]. Hydrogel adhesives are developed to improve the adhesion properties of MN patches by using covalent bonds of surface biomolecules, but only limited to certain types of tissue [30]. The MN patches can also be mechanically fixed to the tissue with bandages and sutures, which may cause tissue damage and increase wound healing time [31]. In nature, many organisms possess excellent surface adhesion ability due to their unique molecular attraction or microstructure on their surfaces [32,33]. The barbs of feline tongues can enhance adhesion strength through mechanical interlocking with the tissues when penetrated [34]. The natural quill tip of the African porcupine contains microscopic

backward-facing barbs shows higher tissue adhesion strength compared to its barbless quill [35]. Inspired by the structure of porcupine quill barbs, a novel porcupine quill-like shape MN patch with hydrogel back patching will be beneficial to fix on the skin for drug penetration through skin tissue.

Oxygen (O_2) is an essential substance for the survival of aerobic organisms, adequate oxygen facilitates wound healing by promoting cell proliferation and tissue remodeling [36,37]. Calcium peroxide (CaO_2) has been reported as an oxygen carrier for tumor therapy and wound repair due to the generation of oxygen and Ca^{2+} by decomposition in aqueous media [38,39]. In this work, a porcupine quill-like multilayer polycaprolactone/polyvinyl pyrrolidone (PCL/PVP) MN with a Cu-doped polyacrylamide (PAM) composite hydrogel as back patching has been designed by the step-by-step template casting method. Anti-diabetic drug (metformin) and sodium hyaluronate-modified CaO_2 nanoparticles (CaO_2-HA NPs) have been encapsulated in the MN for regulation of blood glucose levels and generating O_2 to promote wound healing (Figure 1a). The flexible and adhesive composite hydrogel back patching formed by Cu-doped PAM ensure the MN patches cannot been peeled off from the application sites and reduced bacterial infection. The bio-inspired multilayer MN patches exhibit excellent mechanical and antibacterial properties, which have a potential multifunctional dressing platform for promoting wound healing (Figure 1b).

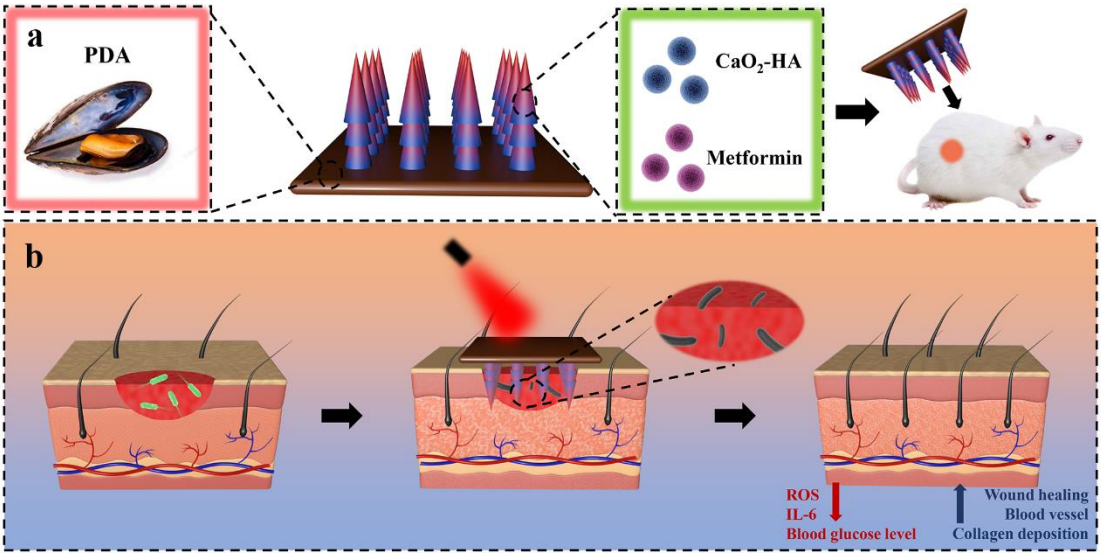

Figure 1 Schematic illustrations of MN patches for diabetic wound healing, (a) schematic structure of MN patches; (b) schematic process for the wound healing using MN patches as dressings.

2. Material and methods

2.1 Materials

Dopamine hydrochloride (DA), polyvinylpyrrolidone (PVP, Mw = 130 kDa) and polycaprolactone (PCL, Mw = 70−90 kDa) were purchased from Mclean Bio-chemical Technology Co., Ltd. (Shanghai, China). Acrylamide (AM, 99.0%), ammonium persulfate (APS, 98.0%), N, N-methylene bisacrylamide (BIS, 98.0%), tetramethylene ethylenediamine (TMEDA, 50%), sodium hyaluronate (NaHA), calcium chloride dihydrate （$CaCl_2{\cdot}2H_2O$, 99%） and cupric chloride ($CuCl_2$, 98%) were purchased from Aladdin Bio-chemical Technology Co., Ltd. (Shanghai, China). 3-(4,5-Dimethyl-2-thiazolyl)-2,5-diphenyl tetrazolium bromide (MTT) was purchased from Beyotime Biotechnology Co., Ltd. (Shanghai, China). All reagents used were of analytical grade and used as received.

2.2 Fabrication of CaO_2-HA NPs

The synthesis procedure of CaO_2-HA NPs was synthesized based on the previous reports with a small modification [40,41]. Typically, NaHA solution (1 mL, 0.5 mg/mL) was firstly added to the mixture of methanol (60 mL) and $CaCl_2$ solution (1 mL, 2 M) under magnetic stirring for 10 min. Then, H_2O_2 (500 μL, 30 %) was added and continued to stir for another 10 min at room temperature. Afterwards, the synthesized CaO_2-HA NPs were precipitated by dropwise of $NH_3 \cdot H_2O$ (25 %) to the above solution until the color of solution changed to be Cambridge Blue. The product was collected after centrifugation and washing with methanol/ethanol for several times. Finally, the CaO_2-HA NPs were obtained after drying.

2.3 Fabrication of porcupine quill-like multilayer microneedle patches

For the preparation of PDA-PAM/Cu^{2+} hydrogel prepolymer, the hydrogel prepolymer solutions were firstly prepared in advance. Dopamine hydrochloride (6.4 mg) was firstly added into alkaline PBS buffer aqueous solution (5 mL, pH = 11) and kept stir at room temperature for 20 min to obtain a black PDA solution. Then, AM (800 mg), APS (80 mg), BIS (4 mg), and $CuCl_2$ (1 mg) were added into the above PDA solution under an ice bath. Finally, the hydrogel was obtained after adding TMEDA (10 μl) for 10 min. The PAM-PDA hydrogel was prepared without adding $CuCl_2$. Identically, PAM or PAM/Cu^{2+} hydrogels were respectively prepared as control samples in the absence of PDA and $CuCl_2$ or PDA.

To mimic the structure of the barbs, the multilayer structure MN patches were fabricated by a step-by-step template casting method, in which each MN exhibited a

porcupine quill-like shape with sharp tips and tiny barbed structure. Briefly, PCL (10 g) as the matrix material of MN was firstly melted at 60 ℃. Then, PVP (2 g), metformin (0.3 g) and CaO_2-HA NPs (20 mg) were added to the molten PCL under magnetic stirring. The certain amount of the melt mixture was poured onto the surface of the PDMS negative mold, which then kept under vacuum for 2 min to fully fill the cavities of mold. The residual melt mixture was removed from the surface of mold by the medicine spoon. Then, the mixture of pre-prepared hydrogel prepolymer solution and TMEDA (as cross-linked agent, volume ratio of hydrogel prepolymer solution and TMEDA controlled at 100,1) was poured on the surface of the PDMS mold, and placed at 25 ℃ for 5 min to form the back patching of MN. Different MN backings can be obtained by adding different hydrogel prepolymer solution. The single-layer MN patches were detached from the mold after curing of the hydrogel. For the fabrication of di-layer structure MN patches, the single-layer MN patches were vertically immersed into half-filled PMDS mold by controlling the immersion depth. Then, the di-layer structure MN patches were fabricated successfully by gently peeling the negative mold off after the curing. The triple-layer structure MN patches were obtained using the same approach by a two-cycle manufacturing process.

2.4 Photothermal effect

For measuring the photothermal conversion performance of the hydrogel, various MN hydrogel back patchings (PAM, PAM/Cu^{2+}, PAM-PDA and PAM-PDA/Cu^{2+}) were irradiated with the NIR laser light (808 nm, 1.6 W/cm^2) for 300 s. Real-time temperature and the thermal image were obtained by an infrared thermal imager (325,

Fotric, America). To further investigate the photothermal stability of the hydrogels, the cyclic irradiation was conducted at the same conditions.

2.5 Tissue adhesion test

Various weights were used to intuitively investigate adhesion properties by tensile adhesion testing. Besides, a universal testing machine was used to quantitatively measure the adhesion of MN patches. MN patches and skin tissue were fixed on the top and bottom of the universal testing machine, respectively. The platform pierces the MN into the skin tissue at a speed of 1 $mm \cdot min^{-1}$. After penetrating the skin completely, the platform retreated in the opposite direction at the same speed, and the maximum separation force of the separation process of the microneedle and the skin tissue was recorded.

2.6 *In vivo* wound healing evaluation

All animal procedures were approved by the Animal Ethics Committee of Zhejiang Sci-Tech University (acceptance number: 2019-02-01) and performed in Zhejiang Yingyang Pharmaceutical R&D Co., Ltd. To establish the infected full-thickness diabetes wound model, the male Sprague-Dawley (SD) rats with an average weight of 200-250 g were allowed to induce as the T2D diabetes model by fasting injection of streptozotocin (STZ, 50 $mg \cdot kg^{-1}$) sodium citrate buffer after being acclimatized for a week. The blood glucose levels (BGLs) were monitored to check the successful establishment of the diabetic model. Diabetic rat models were considered to be successfully induced when the fasting BGLs consistently exceeded 13.9 $mmol \cdot L^{-1}$.

Subsequently, the diabetic rats were randomly divided into seven groups (control group, PAM MN group, PAM/Cu^{2+} MN group, PAM-PDA MN group, PAM-PDA/Cu^{2+} group, CaO_2-HA loaded PAM-PDA/Cu^{2+} MN group, metformin loaded PAM-PDA/Cu^{2+} MN group). Two full-thickness defect wounds open around 1 cm in diameter were created on each side of the spine after the back hair of SD rats was shaved under anesthesia with 3 % pentobarbital sodium (30 $mg \cdot kg^{-1}$).

The wounds of each rat were treated with MN patches (PAM hydrogel-based MN, PAM/Cu^{2+} hydrogel-based MN, PAM-PDA hydrogel-based MN, PAM-PDA/Cu^{2+} hydrogel-based MN) and irradiated with NIR laser light (808 nm, 1.6 W cm^{-2}) for 2 min every 2 days. In the next 12 days, the wound regeneration condition was recorded by a smartphone on day 0, 2, 4, 6, 8, 10 and 12. The Image J software was used to measure wound areas and wound closure of each group was calculated according to follows,

$$\text{Wound closure (\%)} = (1 - (A_t / A_0)) \times 100\%$$

where, A_t and A_0 are the wound areas on day t and day 0, respectively.

2.7 Histological and immunohistochemical analysis

All the rats were sacrificed after 12 days, and the wound site tissue was fixed with Paraformaldehyde solution for 24 h after harvesting the wounds. tissues were embedded in paraffin and transected along with the tissue to 5 μm thick slices. Finally, hematoxylin-eosin (H&E) staining and Masson staining were used to stain the tissue sections. At the same time, immunohistochemical sections stained by CD31 and IL-6

were carried out to confirm the regeneration of blood vessels and evaluated inflammatory responses respectively, by evaluating the expression of CD31 and IL-6. All slices were analyzed and scanned through the scanner.

2.8 Statistical analysis

The Statistical significance analysis of more than two groups was evaluated using one-way ANOVA analysis in Graphpad Prism 7.0 and Origin 2018. A value of $p < 0.05$ (*), 0.01(**), 0.001(***) and 0.0001(****) was considered significant differences. The values were expressed as means ± standard deviation (s. d.).

3. Results and discussion

3.1 Characterization of CaO_2 NPs

To avoid premature degradation of CaO_2 NPs, CaO_2 nanoparticles modified with sodium-hyaluronate (CaO_2-HA NPs) were synthesized in a methanol-water system at room temperature as a previous reported method [41]. Scanning electron microscopy (SEM) and transmission electron microscopy (TEM) were used to observed the morphologies of CaO_2 NPs and CaO_2-HA NPs. As shown in Figure 2a-d, both CaO_2 NPs and CaO_2-HA NPs have the spherical structure with an average size around 50 nm. It can be seen in the TEM image of CaO_2-HA NPs, showing the clear edges of CaO_2 NPs. However, the edge structure of the CaO_2-HA NPs becomes blurred due to the modification of HA. And the size the CaO_2-HA NPs is slightly larger than that of the CaO_2 NPs that conformed by the DLS tests (Figure 2e). In addition, the hydrodynamic size distributions of CaO_2 and CaO_2-HA NPs are narrow. The larger hydrodynamic

diameter of CaO_2-HA NPs could be partially attributed to the hydrogen bonding networks formed by the surface-modified sodium hyaluronate, which is corresponding to the broad absorption peaks at 3600-3200 cm^{-1} in the FTIR spectrum ascribed to the hydrogen bond O-H stretching vibration [40]. Besides, the characteristic peaks presented around 830, 880 and 1115 cm^{-1} are also confirmed the existence of peroxide groups from CaO_2 NPs (Figure 2f). The chemical composition of CaO_2 is further determined by energy-dispersive X-ray (EDS), and the successful synthesis of CaO_2 NPs is further demonstrated by the presence of elements C, O and Ca (Figure 2g). The characteristic diffraction peaks around 2θ = 30.3 °, 35.6 °, 47.31°, 53.2 ° and 60.9° corresponded to the standard reference value for CaO_2 (card NO. 03-0865) [42], which reflecting the successful formation of high crystalline CaO_2 NPs (Figure 2h). Efficient modification of CaO_2 NPs by sodium hyaluronate can be ascribed to the static attraction between negatively charged ions of sodium hyaluronate and positive surface charges of CaO_2 NPs. As shown in Figure 2i, the zeta potential of CaO_2-HA NPs decreased by about 12 mV compared to the CaO_2 NPs before modification.

As a promising O_2 carrier, CaO_2 can be decomposed to produce H_2O_2 which possesses excellent antibacterial effect and can be further decomposed to produce O_2. The H_2O_2 produced by the hydrolysis of CaO_2 NPs can reduce the $KMnO_4$ solution from purple-red to transparent, which can be used to assess the antioxidant capacity of CaO_2 NPs and CaO_2-HA NPs [43]. As shown in Figure S1a, after adding CaO_2 NPs (100 μg/mL) into $KMnO_4$ solution (50 μg/mL), the characteristic peaks at 545 and 525 nm of $KMnO_4$ solution in the UV-Vis spectra are disappeared. And the solution is faded to

colorless within 5 min, indicating the rapid hydrolysis CaO_2 NPs and its excellent antioxidant capacity. However, the $KMnO_4$ solution with CaO_2-HA NPs (100 μg/mL) shows a slight decrease of characteristic peaks within 5 min and fades to colorless after 1 h, indicating better stability of CaO_2-HA NPs (Figure S1b).

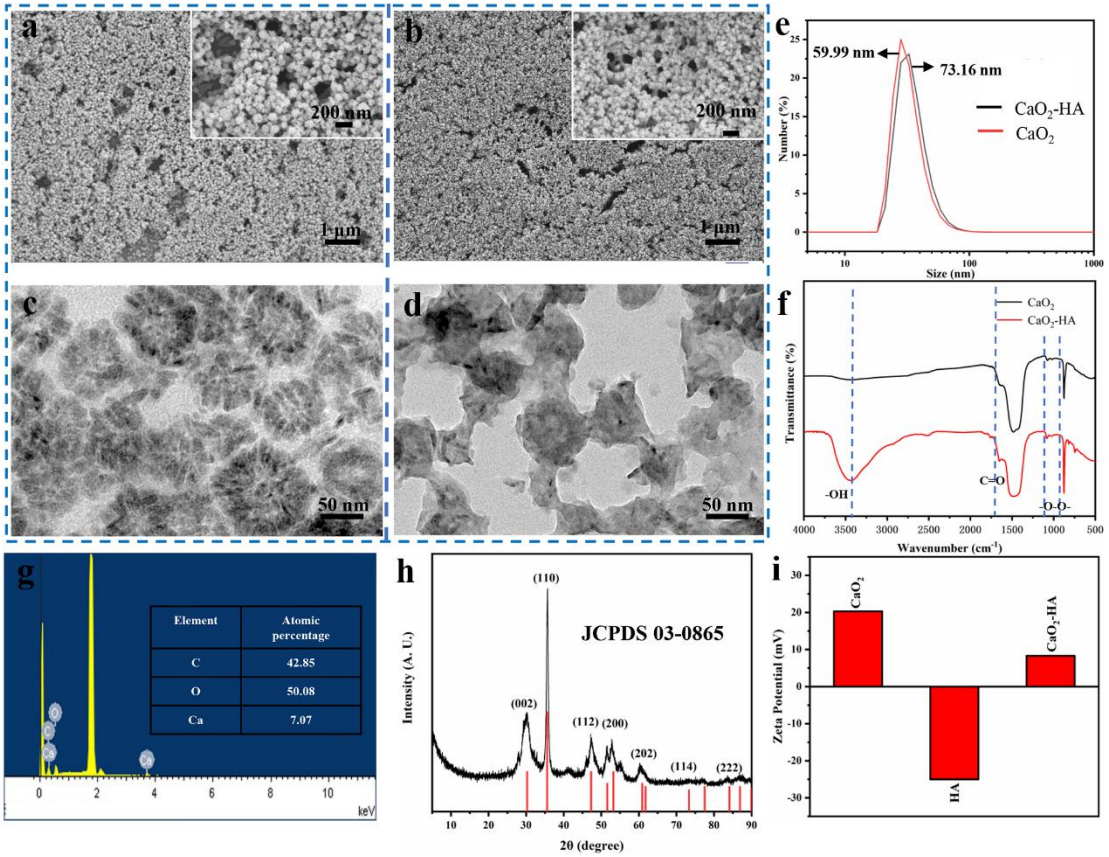

Figure 2 SEM images of CaO_2-HA (a) and CaO_2 (b) NPs, TEM images of CaO_2-HA (c) and CaO_2 (d) NPs, DLS of CaO_2-HA and CaO_2 (e) NPs, infrared spectra of CaO_2-HA and CaO_2 NPs (f), EDS of CaO_2-HA NPs (g), XRD of CaO_2-HA NPs (h) and Zeta potential of CaO_2-HA and CaO_2 (i) NPs.

3.2 Preparation and physicochemical characterization of hydrogels

The composite hydrogel MN backings are produced by a two-step process [44-45]. Polydopamine (PDA) is firstly obtained by inducing pre-polymerization under alkaline conditions. Then, the PAM-PDA/Cu^{2+} hydrogel is prepared by an aqueous radical polymerization. The photothermal stability and antibacterial activities are improved by

the introduction of Cu^{2+}. FTIR spectrometry is used to further verify possible crosslinking in the obtained hydrogel backing. As shown in Figure 3a, the new peak at 1260 cm^{-1} can be found in the spectra of PAM-PDA and PAM-PDA/Cu^{2+} hydrogel, which could be ascribed to the stretching vibration of C-N [45]. It is worth noting that the interaction between amino groups in PAM and phenolic hydroxyl groups in PDA is indicated by the appearance of the new peak. The PAM, PAM/Cu^{2+} and PAM-PDA MN hydrogels backings are also prepared using the similar method (Figure S2a).

The morphologies of the as-fabricated hydrogel MN back patching are observed by SEM. As shown in Figure 3b-e, all MN back patching exhibit porous structures and the corresponding pore size distributions are also calculated according to SEM images by Image J. The average pore diameters of PAM, PAM/Cu^{2+}, PAM-PDA and PAM-PDA/Cu^{2+} hydrogel MN back patchings are 10.01, 9.82, 18.12 and 22.30 μm. The porosity of PAM-PDA and PAM-PDA/Cu^{2+} hydrogel MN back patchings are 42.74% and 41.93%, which are smaller than PAM (51.79%) and PAM/Cu^{2+} (52.28%) hydrogel MN back patchings (Figure 3f). Compared with smooth surfaces of PAM hydrogel MN back patchings, the composite hydrogel MN back patchings containing PDA have a microfibril structure. These microfibril structure can be attributed to the mutual diffusion of PAM and PDA chains through π-π interactions and hydrogen bonds [45]. The equilibrium swelling ratio of hydrogel MN back patchings containing PDA is dropped to ~600 % compared to that of hydrogel MN back patchings without PDA (~750%), which can be contributed to higher crosslinking density between of PAM and PDA (Figure 3g). The high equilibrium swelling ratio of hydrogel MN back patchings

is beneficial to the absorbing wound tissue exudate, indicating its application prospect in wound healing dressing. The adhesion and flexibility of the hydrogel MN back patchings can afford the MNs better adhesion to the skin at various angles [46]. In addition, the adhesive MN patches make it possible to completely adhere and combine with the tissues, which can avoid infections and promote healing by providing a beneficial microenvironment. The hydrogel MN back patchings exhibit excellent adhesion when applied to various material surfaces (such as, hydrophilic, hydrophobic, plastic, metallic, and organic tissues). Meanwhile, the weight of adhesive support can reach 100 g (Figure S2b). PAM-PDA/Cu^{2+} hydrogel MN back patchings also can be firmly applied to the wrist joint even if it is bent to different angles (Figure 3h). The excellent of adhesion and flexibility properties offer hydrogel MN back patchings have application prospect in wound healing by extending the effective the service life of hydrogel and preventing the infection of the wound and falling off from skin even when it is applied on the dynamic wound.

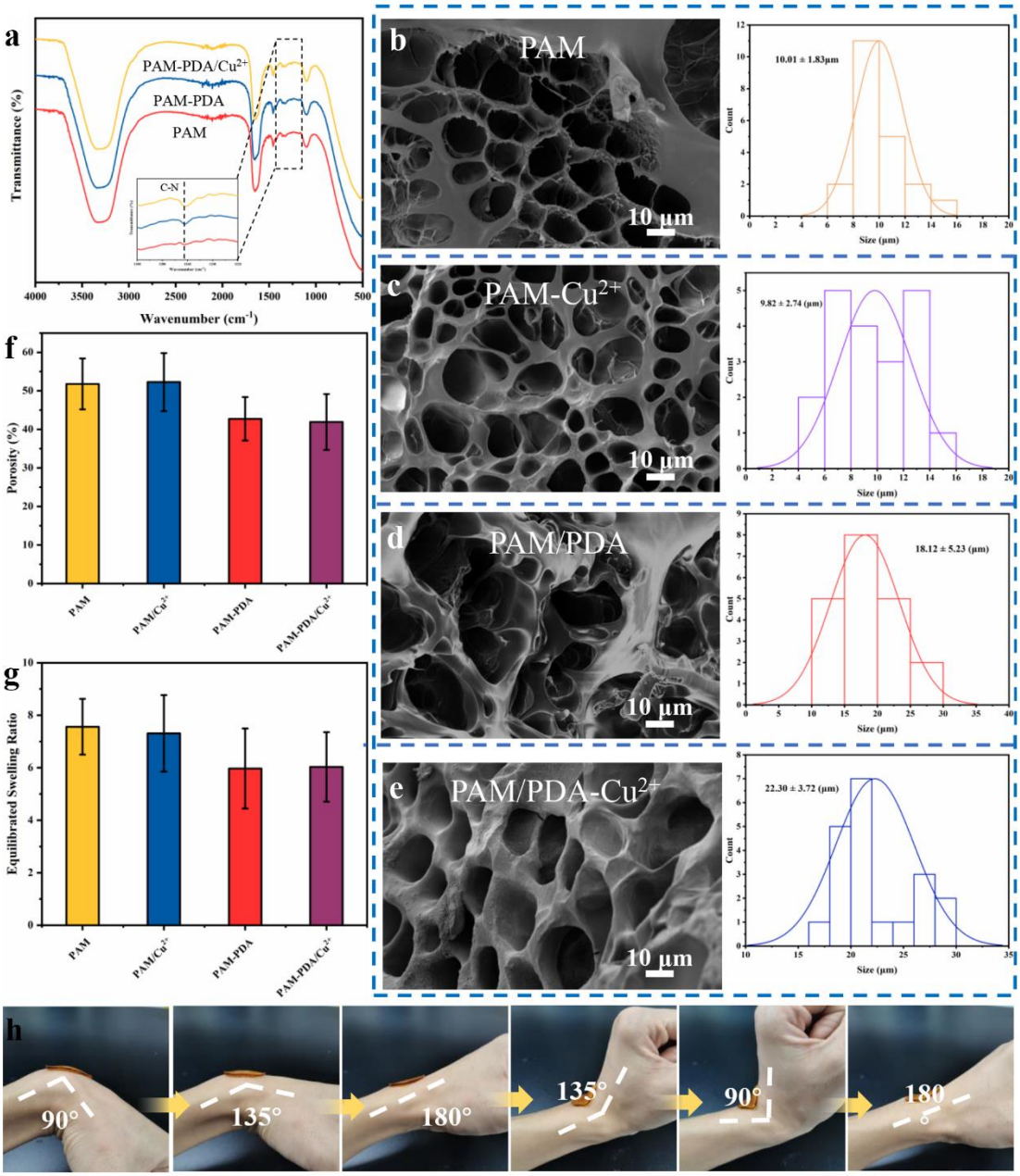

Figure 3 Infrared spectra of the PAM, PAM-PDA, and PAM-PDA/Cu^{2+} hydrogels (a), SEM images of PAM (b), PAM/Cu^{2+} (c), PAM-PDA (d) and PAM-PDA/Cu^{2+} (e) hydrogel back patchings. Porosity of hydrogel back patchings (f). Equilibrated swelling ratio of hydrogel back patchings (g). Adhesion effect of the PAM-PDA/Cu^{2+} hydrogel back patching on human wrist during exercise (h).

3.3 Fabrication of multi-layer structure MN patches

Porcupine's quills can pierce the skin of enemies and make them difficult to shed. As shown in Figure S3a and b, the microscopic barb structures in the black region of porcupine quill can be found on the surface, which enhanced penetration and

application to skin tissue, the porcupine quill can drag the pig skin during the lifting process, which shows more vital subcutaneous stagnation ability compared with the barbless needle (Figure S3c). In this study, multi-layer structure MNs with composite hydrogel back patching was fabricated by a layer-by-layer stacking using mold technology (Figure 4a). The melt needle matrix is firstly coated on the surface of MN mold and filled the mold cavity under negative pressure. After removing the residual matrix on the surface of mold, the hydrogel prepolymer solution is poured into mold. The single-layer MN patch is obtained after curing of hydrogel prepolymer. The di-layer structure MN patch is fabricated by vertically immersion of the single-layer MN patch into MN mold PMDS mold preloaded with half-filled melt needle matrix. And the tri-layer structure MN patch is fabricated through 2 immersion cycles using the same route. Digital microscope images of MN and fluorescence images of MN section taken by laser confocal microscope are shown in Figure 4b-c. It can be found that the barb-like structure is created due to extra area generated at the junction of two adjacent layers of MN, which may enhance MN adhesion after piercing into the skin.

As shown in Figure 4d, it can be observed that the multi-layer structure MN show uniform heights and layer spacing. The heights and layer spacing of the MN can be adjusted by regulation the amount and height of melt needle matrix in the preloaded PMDS mold which offer a feasible method to control the morphology and high of multi-layer structure MN patches.

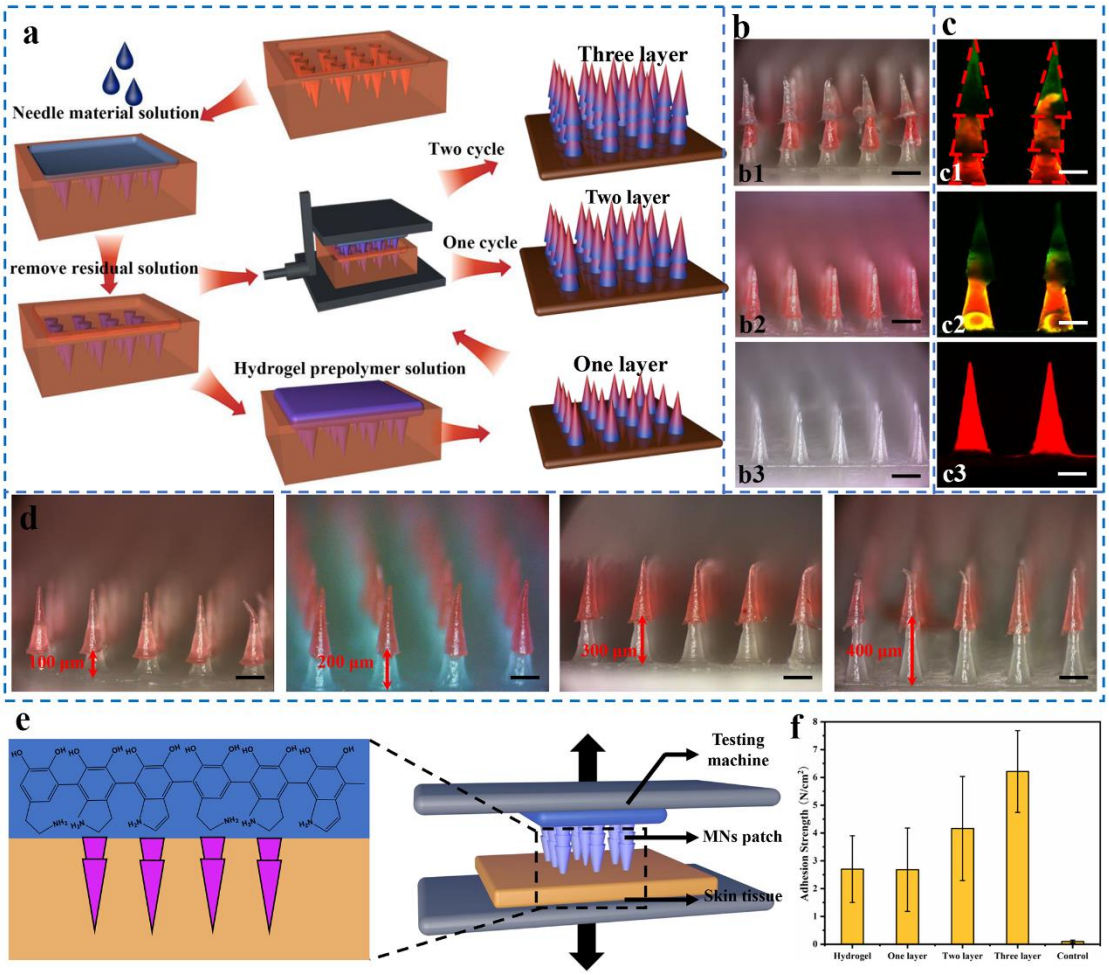

Figure 4 Schematic illustration for the fabrication process of multi-layer structure MN patches (a). Digital microscopy images (b) and section fluorescence images (c) of single-layer, double-layer, and triple-layer structure MN patches, scale bars, 250 μm. Di-layer microneedles with a layer spacing of 100, 200, 300, and 400 μm, scale bars, 250 μm (d). Schematic illustration of MNs patch adhesion experiment (e) and maximum detachment forces of single-layer, double-layer, and triple-layer structure MN patches (f).

The porcupine quill-like multilayer MN patches that can be effectively adhered to the skin surface by the synergy of microstructure of MNs and adhesion of MN back patching, which facilitates drug delivery through transdermal route. The adhesion strength of the MN patches to representative skin tissue is quantified by a universal testing machine (Figure 4e). The highest adhesion strengths to skin tissue of PAM-PDA/Cu^{2+} hydrogel, single-layer MN, double-layer MN and triple-layer MN are 2.71,

2.70, 4.14 and 6.21 N/cm^2, respectively (Figure 4f). The adhesion of the hydrogel MN back patching is caused by hydrogen bonds produced by amide group of PAM and skin tissue. In addition, the catechol groups in PDA also can form hydrogen and covalent bonds with the skin tissue, which further enhances the adhesion of hydrogel MN back patching. The adhesion of di-layer MN and tri-layer MN can be further improved, which confirms the synergy of microstructure of MNs and adhesion of MN back patching. Furthermore, MN patches are well stretched and twisted without crack, indicating the excellent flexibility of the MN back patching, as shown in Figure S4.

3.4 Photothermal performance of the composite hydrogel MN backing

The local temperature enhancement generated by the photothermal effect can inhibit bacteria, reduce the inflammatory response, and promote wound healing [47,48]. To evaluate the photothermal effect of the hydrogel MN back patching, they are exposure to NIR laser. Photothermal images at different times and corresponding temperatures are recorded with an infrared thermal imager. As shown in Figure 5a, after NIR irradiation for 180 s, the temperatures of PAM-PDA and PAM-PDA/Cu^{2+} hydrogel MN back patchings are significantly higher than the temperatures of PAM and PAM/Cu^{2+} hydrogel MN back patchings. PAM-PDA and PDA-PAM/Cu^{2+} hydrogel MN back patchings show a temperature increase of 28.5℃ and 46.8 ℃ compared with PAM hydrogel MN back patching after NIR irradiation for 300 s, which is significantly higher than that of PAM-Cu^{2+} hydrogel MN back patching (12.9 ℃) (Figure 5b). The results indicate that PDA has excellent photothermal conversion efficiency, and Cu^{2+} also enhances the photothermal performance of the hydrogel MN back patching. In

order to further determine the photothermal stability of the hydrogel MN back patching, the photothermal cycle curves of them are obtained by periodically switching the laser on and off. As shown in Figure 5c, the temperature of PAM-PDA/Cu^{2+} hydrogel MN back patching rapidly rises to 50 °C within 30 s after switching on the laser. And the temperature rapidly dropped to room temperature after switching off the laser. The photothermal conversion ability of PAM-PDA/Cu^{2+} MN back patching can still be maintained after 5 on/off cycles.

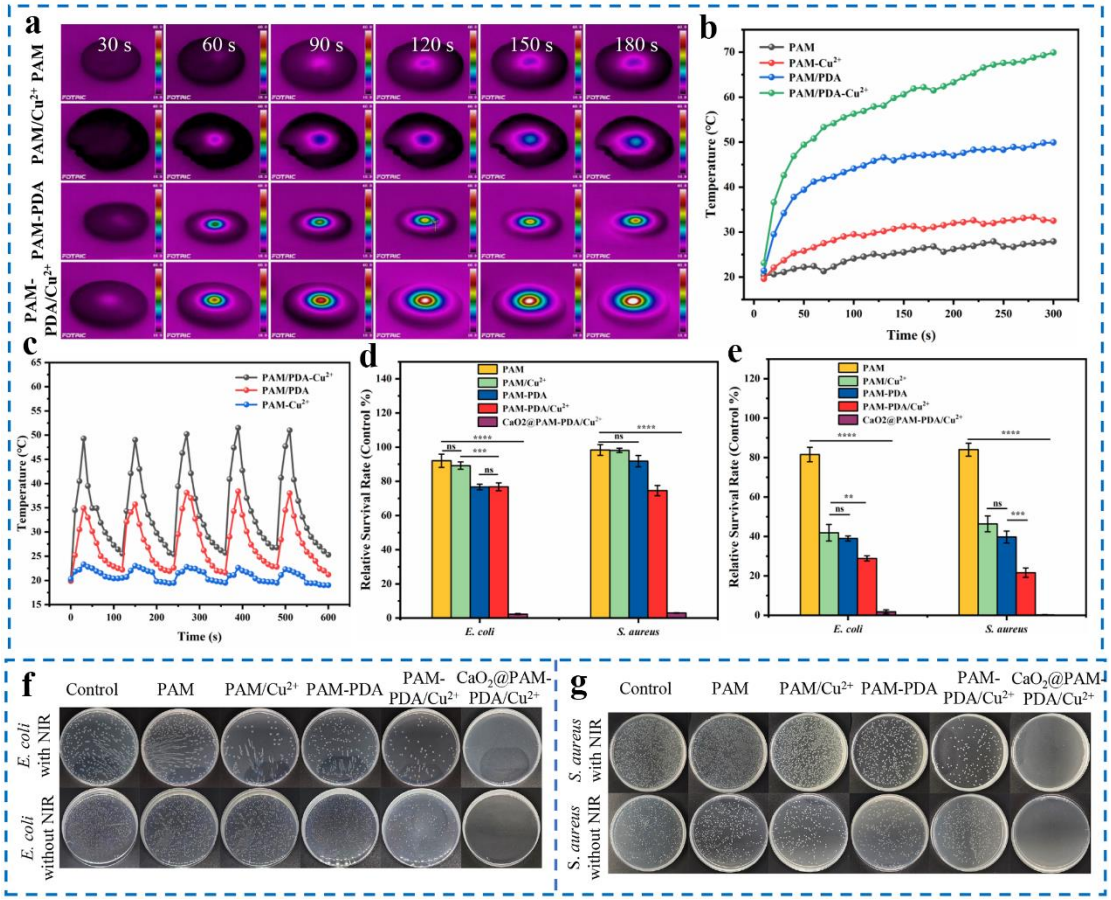

Figure 5 Photothermal conversion performance and antibacterial effects of the hydrogel back patchings. Infrared thermographic images of different hydrogel back patchings (a). Photothermal curves of different hydrogel back patchings (b), cyclicity curves of different hydrogel back patchings for photothermal conversion (c). The survival rate of *E. coli* and *S. aureus* after treatment by different hydrogel back patchings in the presence and absence of NIR irradiation (d and e). Images of *E. coli* (f) and *S. aureus* (g) after treatment by different hydrogel back patchings.

3.5 Antibacterial performances of MN patch

To determine the antibacterial ability of hydrogel MN back patching against *E. coli* and *S. aureus*, the antibacterial situations are studied by the plate count method. And bacterial survival is calculated by counting the number of colonies. Without NIR light irradiation, the survival rates of *E. coli* and *S. aureus* in hydrogel MN back patchings are more than 80% (Figure 5d). However, after 10 min of NIR exposure, PAM-PDA and PAM-PDA/Cu^{2+} hydrogel MN back patching shows a good antibacterial efficacy. The survival rates of PAM-PDA hydrogel MN back patching against *E. coli* and *S. Aureus* could be decreased to 40.1% and 42.5%. And 28.86% and 21.65% survival rates for PAM-PDA/Cu^{2+} hydrogel MN back patching, much lower than PAM and PAM-PDA hydrogel MN back patchings, implying a synergized photothermal antibacterial activity under NIR irradiation (Figure 5e). These results are further visually verified and shown in Figure 5f and g. The hydrogel MN back patchings containing Cu^{2+} exhibit better antibacterial ability compared to the those without Cu^{2+}. It may be contributed to the effect of Cu^{2+} on the surface of bacteria, which can damage the membrane of bacteria to achieve antibacterial effects [49]. More interesting, CaO_2-HA NPs exhibits excellent antibacterial properties with or without NIR light. Almost all bacteria can be killed, which is consistent with the above result, producing of H_2O_2 due to the decomposition of CaO_2-HA NPs. Taking together, PDA-PAM/Cu^{2+} exhibits an improved antibacterial activity through the synergistic effect of photothermal, Cu^{2+} and CaO_2-HA NPs.

3.6 Cytocompatibility evaluation

Cytocompatibility of dressings is critical for wound healing. The biocompatibility of CaO_2-HA NPs and hydrogel MN back patchings are evaluated by MTT assay. As shown in Figure 6a, the cell viability is over 90% when the concentration of CaO_2-HA NPs ranged from 0 to 250 $\mu g \cdot mL^{-1}$. And the cell viability is still more than 80% even the concentration of CaO_2-HA NPs reached to 1,000 $\mu g \cdot mL^{-1}$, indicating the excellent cytocompatibility of CaO_2-HA NPs against 3T3 cells. All cell viabilities are higher than 80% after co-culture with hydrogel MN back patchings for 24 h, confirming the good biocompatibility of hydrogel MN back patchings (Figure 6b). In addition, cell scratch tests are carried out to semi-quantitative asses the effect of the hydrogel MN back patching on cell migration and proliferation. As shown in Figure 6c and d, the scratch areas are decreased in all groups after 24 h of cell co-culture. The PAM-PDA/Cu^{2+} group (51.77%) shows the smallest scratch area than PAM (86.09%), PAM-Cu^{2+} (71.63%), and PAM-PDA (68.47%) groups, implying that PAM-PDA/Cu^{2+} hydrogel MN back patching suitable for the cell migration and proliferation.

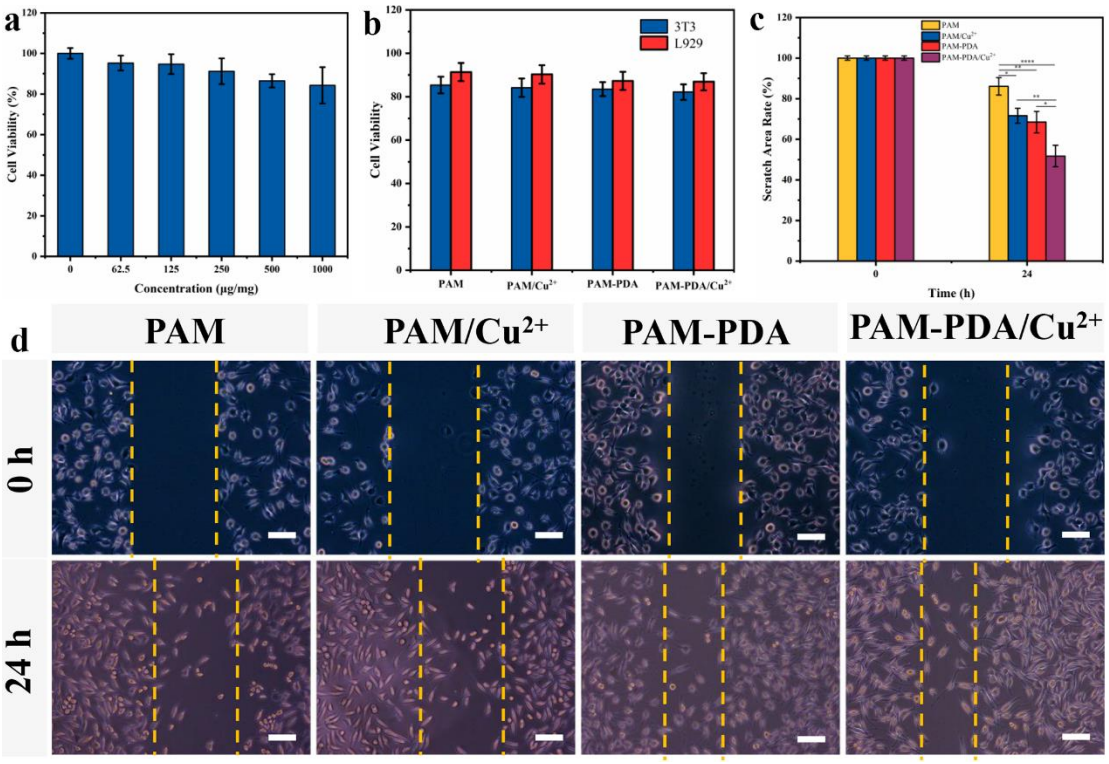

Figure 6 Cells viability of 3T3 cells after treated by CaO_2-HA NPs for 24 h (a), cell viability of 3T3 and L929 cells after co-culture with different hydrogel back patchings (b). Quantitative analysis of the relative scratch area of L929 cells at 0 h and 24 h (c), corresponding images of the scratch area of L929 cells treated by hydrogel back patchings, scale bars,100 μm (d).

3.7 Wound healing *in vivo*

The effect of the MN patches with an adhesive back patching as dressing for wound healing is evaluated *in vivo*. Firstly, a rat model of full-thickness skin defect (1 cm in diameter) is established on the back of the diabetes rats, as shown in Figure 7a. The SD rats are randomly divided into 7 groups after successful modeling, (I) control group (without any treatment), (II) PAM group (with metformin and CaO_2-HA in the tri-layer MN patch), (III) PAM/Cu^{2+} group (with metformin and CaO_2-HA in the tri-layer MN patch), (IV) PAM-PDA group (with metformin and CaO_2-HA in the tri-layer MN patch), (V) PAM-PDA/Cu^{2+} group (with metformin and CaO_2-HA in the tri-layer MN patch), (VI) PAM-PDA/Cu^{2+} group (without metformin but with CaO_2-HA in the

tri-layer MN patch), (VII) PAM-PDA/Cu^{2+} group (without CaO_2-HA but with metformin in the tri-layer MN patch). The MN patches are replaced every 2 days. In Figure S5, the adhesive back patching contained PDA and Cu^{2+} have excellent photothermal properties, the temperature can be raised to a suitable temperature to inhibit bacterial growth and promote wound healing irradiated by NIR light.

The corresponding images of the wounds with different treatment schemes at scheduled time intervals are recorded in Figure 7b. The group V (PAM-PDA/Cu^{2+} group) with metformin and CaO_2-HA in MNs shows a much higher wound healing efficacy than the other groups, and no obvious wounds can be observed after a 12-day treatment. The schematic diagram of skin wound size change during 12-day treatment for different groups is shown in Figure 7c. And the quantitative wound areas and wound closure are calculated based on the wound photographs (Figure 7d and e). After treatment for 2 days, the wound area and wound closure in PDA-PAM/Cu^{2+} group are 64.19% and 35.81%, significantly superior to control (85.68% and 14.32%), PAM (88.82% and 11.18%), PAM-Cu^{2+} (86.59% and 13.41%), and PAM-PDA (70.21% and 29.49%). On day 6, the wound area in PDA-PDA-PAM/Cu^{2+} group is ~10.77%, much lower than that of control (59.43%), PAM (47.96%), PAM-Cu^{2+} (41.79%), and PAM-PDA (32.45%). And the wound closure in PDA-PDA-PAM/Cu^{2+} group is increased to ~90%, much higher than that of control (40.57%), PAM (52.04%), PAM-Cu^{2+} (58.21%), and PAM-PDA (67.55%). Almost no wound area can be detected after 10 days of treatment in PDA-PAM/Cu^{2+} group. On the 12th day, all wounds in PDA-PAM/Cu^{2+} group are completely cured, showing a significant difference in wound closure of control

(83.35%), PAM (89.25%), PAM-Cu^{2+} (95.39), and PAM-PDA (98.80%). The excellent wound healing ability PDA-PAM/Cu^{2+} group can be attributable to the fact that hydrogel back patching provide a consistently moist environment conducive to healing [50]. In addition, the antibacterial effect provided by the PDA and Cu^{2+} from hydrogel back patching and CaO_2-HA NPs from MNs are also accelerated the process of skin wound healing [51-54].

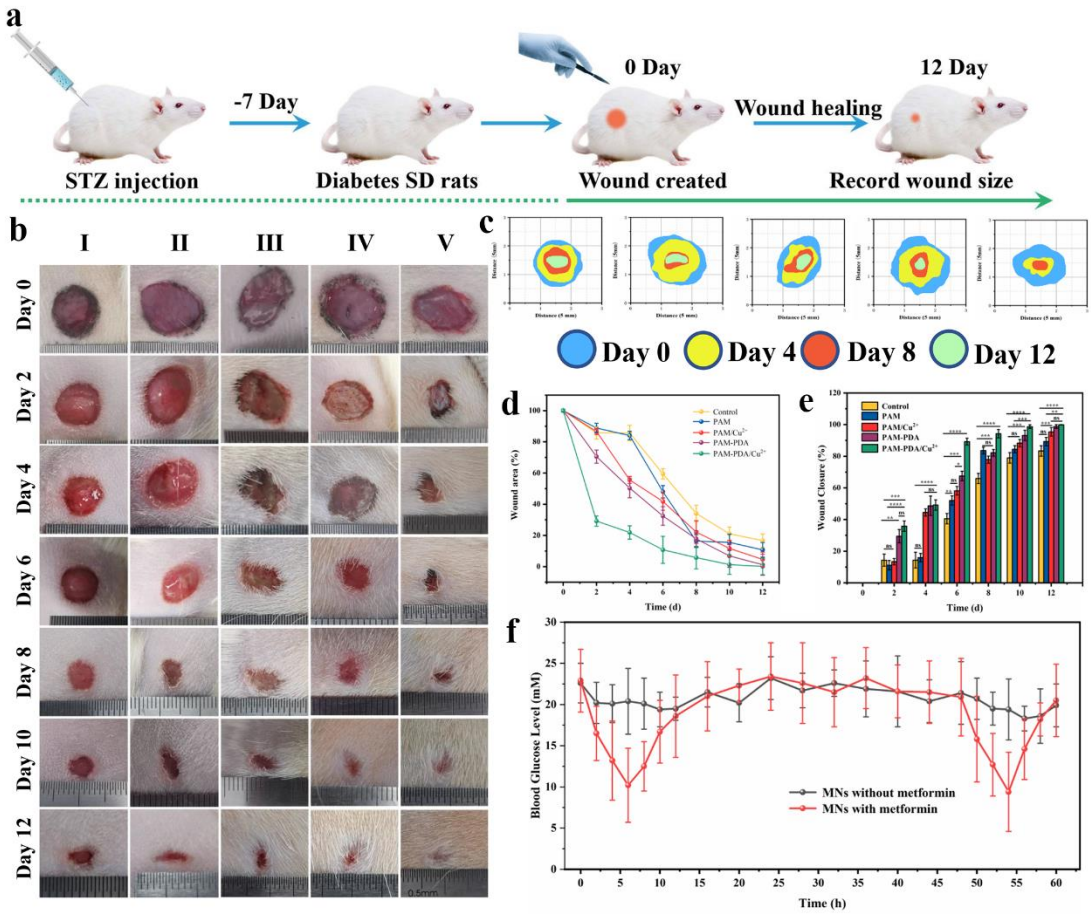

Figure 7 Strategy of multi-layer structure MN patches in the treatment of wounds in diabetic rats (a). The images of wound after treatment by tri-layer structure MN patches at days 2, 4, 6, 8, 10 and 12 (b), and corresponding wound healing trajectory (c). Wound area (d) and wound closure (e) after treatment by the tri-layer structure MN patches. The changes of blood glucose levels of diabetic rats treated by MN patches with and without anti-diabetic drug (f).

The healing of diabetic wound is a complicated process influenced by multiple factors [55]. To evaluate the effect of anti-diabetic drug (metformin) and oxygen donor (CaO_2) on wound healing, the MN patches without metformin but with CaO_2-HA NPs in MNs and with metformin and without CaO_2-HA in MNs are prepared and applied on the diabetes wound. The blood glucose levels can be decreased to minimum level at ~ 10 mM after application of MN patches with metformin (loaded drug 50 mg) for 5 h, and then it is gradually increased to initial level after 15 h, showing a sustained hypoglycemic effect (Figure 7f). Representative wound images treated by MN patches without metformin but with CaO_2-HA NPs, and with metformin and without CaO_2-HA at scheduled time intervals are shown in Figure S6a. The MN patches also are replaced every 2 days. Typically, the wound treated by MN patch with anti-diabetic drug can be accelerated closure at the initial stage of wound healing in compared with control group without any treatment. However, the healing of the wound is faster for the MNs patch with only containing of CaO_2-HA NPs. The wound closures in the MNs patch groups with only containing of CaO_2-HA NPs are ~34.45 and 48.77% after treatment of 2 and 4 days, compared with ~13.59 and 47.74% in the MNs patch groups with only containing of metformin as shown in Figure S6b. After 12-day treatment, the wound closure in the MNs patch groups with only containing of CaO_2-HA NPs and metformin are ~95% and 88% in comparison with control group at ~80% and MNs patch groups with CaO_2-HA NPs and metformin at 100%. It implies that both hypoglycemic effect of metformin and CaO_2-HA play a significant role in wound healing, and oxygen supply and wound microenvironment are more beneficial for wound healing. In addition, the

Ca^{2+} generated by hydrolysis of CaO_2-HA NPs can promote collagen deposition during wound healing [56-58].

Histological analysis is applied to further evaluate the therapeutic effect of the MN patch on the process of wound healing. H&E staining images of rat skin wound tissue slices in each group collected on day 12 are shown in Figure 8a, more neutrophil infiltration could be observed in the control and PAM MN groups. However, Fewer inflammatory cells and smaller wound width could be found in the PAM-PDA/Cu^{2+} MN group relative to the control group, which is consistent with the wound healing results. In addition, more hair follicles and glands also can be found in the PAM-PDA/Cu^{2+} MN group in compared with the other groups.

The deposition of collagen plays an important role in wound healing by rebuilding the skin's tensile strength, which is assessed through Masson staining [59]. The wound surface treated by the PAM-PDA/Cu^{2+} group exhibit more ordered collagen deposition, as shown in Figure 8a. More collagen fibers are found in the PAM-PDA/Cu^{2+} and PAM-PDA groups compared with the control and PAM groups. In Figure 8b, the deposition of collagen are quantitatively analyzed according to the Masson staining section statistics, which confirm that collagen deposition in the PAM-PDA/Cu^{2+}group (55.92%) is significantly higher than that in control (29.57%), PAM (35.34%), PAM/Cu^{2+} (38.16%) and PAM-PDA groups (43.92%). As a transmembrane glycoprotein expressed in the early stage of angiogenesis, CD31 is used to evaluate the existence of vascular endothelial cell tissue and evaluate the effect of angiogenesis on wound healing [60]. As shown in Figure 8c and e, the wound treated by PAM-PDA/Cu^{2+} and

PAM-PDA groups show higher CD-31 positive expression than that of control, PAM and PAM/Cu^{2+} groups, which is beneficial in promoting angiogenesis during wound healing.

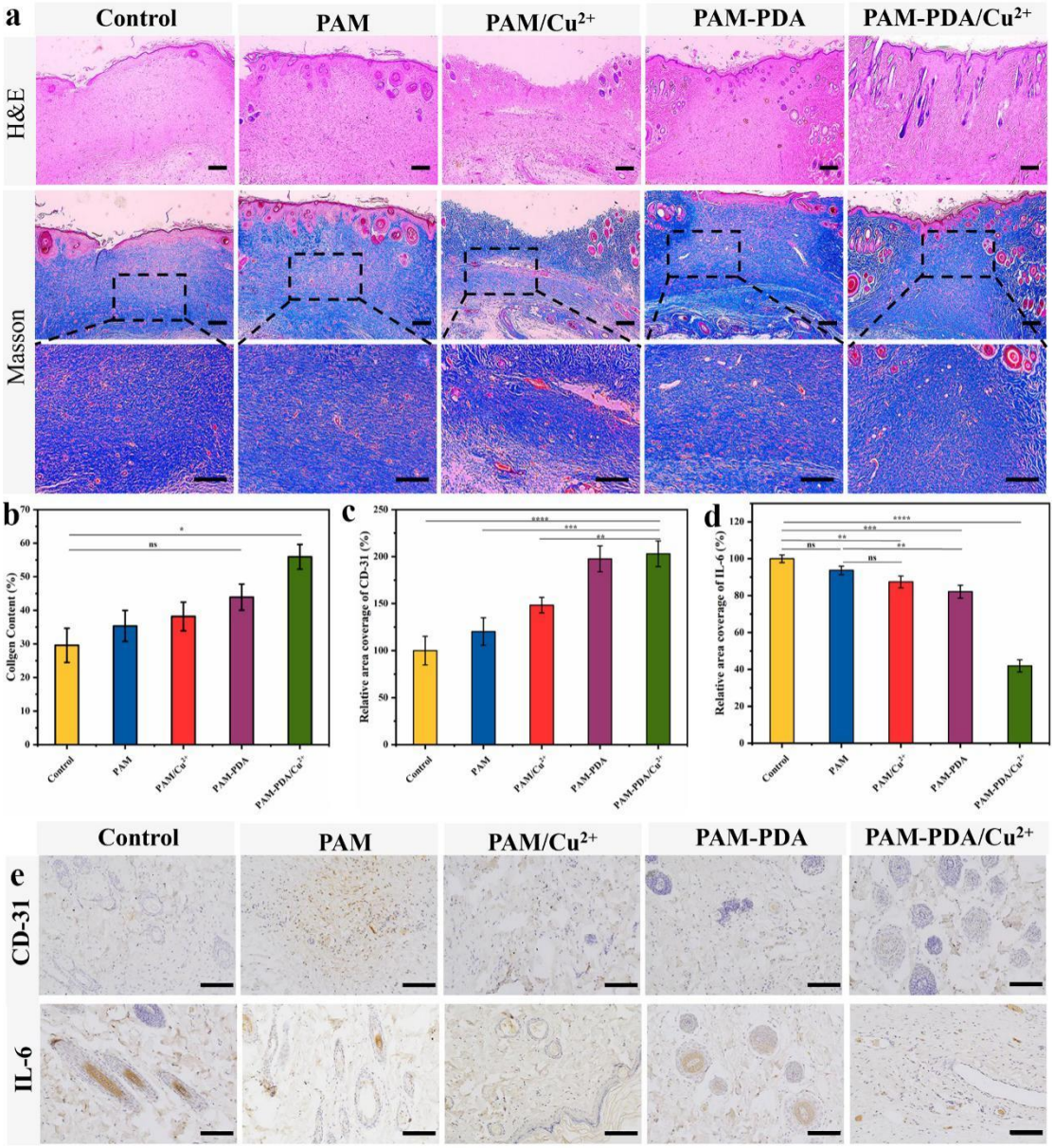

Figure 8 H&E and Masson's staining images of wound tissue after treatment for 12 days, scale bars, 50 μm (a). The collagen content (b), relative area coverage of CD-31(c) and relative area coverage of IL-6 after treatment for 12 days (d). CD-31 and IL-6 immunohistochemical staining images of wound tissue after treatment for 12 days, scale bars, 100 μm (e).

To further investigate the wound healing mechanism, the inflammatory response

to wound treatment is assessed by IL-6 immunohistochemical staining [61]. Overexpression of IL-6 indicates an exacerbation of the inflammatory response, which will hinder the wound healing process. As shown in Figure 8 d and e, immunohistochemical staining of IL-6 shows that the inflammatory level can be significantly inhibited by treatment of PAM-PDA/Cu^{2+} group. Taking together, the PAM-PDA/Cu^{2+} MN patches loaded with CaO_2-HA NPs and metformin has the best anti-inflammatory activity, antioxidant capacity, and angiogenic properties, which has a potential application in accelerating diabetic wound healing.

4. Conclusion

In this study, we designed a porcupine quill-like multilayer MN patch with an adhesive back patching for tissue adhesion and diabetic wound healing. The oxygen donor (CaO_2-HA NPs) and hypoglycemic agent (metformin) were loaded into the needle-tips of MNs, endowing them with exceptional antibacterial ability and hypoglycemic effect. The flexible and adhesive back patching ensured the MN patches could not been peeled off from the application sites and reduce bacterial infection. In addition, the local temperature of the skin tissue could be improved under NIR irradiation due to the outstanding photothermal effect of PDA, resulting in the efficient antibacterial effect. Immunological analysis showed that the as-fabricated MN patches had a synergistical effect for accelerating wound healing by integration of CaO_2-HA NPs and metformin, inhibiting inflammation at the wound sites while promoting angiogenesis during the wound healing process, showing a potential application potential in various related medical fields.

Author information

Corresponding Authors

Guohua Jiang − *Department of Polymer Materials, School of Materials Science and Engineering, Zhejiang Sci-Tech University, Hangzhou, Zhejiang 310018, China; Zhejiang-Mauritius Joint Research Center for Biomaterials and Tissue Engineering, Zhejiang Sci-Tech University, Hangzhou, Zhejiang 310018, China; Institute of Smart Biomedical Materials, Zhejiang Sci-Tech University, Hangzhou, Zhejiang 310018, China*; Phone: +86 571 86843527; orcid.org/0000-0003-3666-8216; Email: ghjiang_cn@zstu.edu.cn

Yanfang Sun − *College of Life Science and Medicine, Zhejiang Sci-Tech University, Hangzhou, Zhejiang 310018, China*; Email: katherineyfs@zstu.edu.cn

Authors

Tianqi Liu − *School of Materials Science and Engineering, Zhejiang Sci-Tech University, Hangzhou, Zhejiang 310018, China; International Scientific and Technological Cooperation Base of Intelligent Biomaterials and Functional Fibers, Hangzhou, 310018, China*

Wenjing Zhang - *School of Materials Science and Engineering, Zhejiang Sci-Tech University, Hangzhou, Zhejiang 310018, China; International Scientific and Technological Cooperation Base of Intelligent Biomaterials and Functional Fibers, Hangzhou, 310018, China*

Rui Wang *- School of Materials Science and Engineering, Zhejiang Sci-Tech University, Hangzhou, Zhejiang 310018, China; International Scientific and Technological Cooperation Base of Intelligent Biomaterials and Functional Fibers, Hangzhou, 310018, China*

Khaydar E. Yunusov *- Institute of Polymer Chemistry and Physics, Uzbekistan Academy of Sciences, Tashkent, 100128, Uzbekistan*

Uladzislau E. Aharodnikau *–Research Institute for Physical Chemical Problems of the Belarusian State University, Minsk, 220030, Belarus*

Sergey O. Solomevich *- Research Institute for Physical Chemical Problems of the Belarusian State University, Minsk, 220030, Belarus*

Lei Nie *- BioMatter unit-École polytechnique de Bruxelles, Université Libre de Bruxelles, Brussels, Belgium; College of Life Sciences, Xinyang Normal University, Xinyang 464000, China*

Amin Shavandi *- BioMatter unit-École polytechnique de Bruxelles, Université Libre de Bruxelles, Brussels, Belgium*

Author contributions

T. L., W. Z. and R. W. produced microneele patch samples and performed cell and animal experiments; T. L., R. W. and G. J. analyzed the results and wrote the draft of manuscript; G. J. and Y. S. conceived the idea and designed the experiments; K. E. Y., U. E. A. and S. O. S. analyzed the results and review the manuscript; L. N. and A. S.

provided suggestions and commented on the manuscript.

Declaration of Competing Interest

The authors declare that they have no known competing financial interests or personal relationships that could have appeared to influence the work reported in this paper.

Acknowledgments

This work was financially supported by the National Natural Science Foundation of China (51373155, 51873194) and the Natural Science Foundation of Zhejiang Province (LY18E030006).

Tianqi Liu is currently a PhD student at Department of Polymer Materials, College of Materials Science and Engineering, Zhejiang Sci-Tech University. His research focuses on transdermal delivery using polymer microneedles.

Guohua Jiang received BSc and MSc degrees from Hangzhou Normal University in 1999 and 2003, respectively, and a PhD degree (in polymer chemistry) from Zhejiang University in 2006. He worked as a post-doctoral researcher at Nanyang Technological University, Singapore and University of Michigan, USA from 2006 to 2008. He is currently a professor at Zhejiang Sci-Tech University. His research interests include multifunctional biomaterials as well

as their applications in drug delivery and wound healing.

REFERENCES

[1] R. Augustinea, A. Hasana, Y. B. Dalvi, S. R. Ur Rehman, R. Varghese, R. N. Unni, H. C. Yalcin, R. Alfkey, S. Thomas, A. A. Moustafa. *Mater. Sci. Eng. C*, **2021**, 118, 111519.

[2] B. S. Shailendra, M. Rishabha, *Endocr. Metab. Immune Disord - Drug Targets*, **2022**, 22, 911.

[3] M. M. Ghaisas, S. B. Kshirsagar, R. S. Sahane, *Int. Wound J.*, **2014**, 11, 523.

[4] X. Peng, X. Xu, Y. Deng, X. Xie, L. Xu, X. Xu, W. Yuan, B. Yang, X. Yang, X. Xia, L. Duan, L. Bian, *Adv. Funct. Mater.*, **2021**, 31, 2102583.

[5] Y. Ding, Z. Sun, R. Shi, H. Cui, Y. Liu, H. Mao, B. Wang, D. Zhu, F. Yan, *ACS Appl. Mater. Interfaces*, **2019**, 11, 2860-2869.

[6] V. T. Le, T. X. X. Trinh, P. N. Chien, N. N. Giang, X. Zhang, S. Nam, C. Heo, *Polymers*, **2022**, 14, 919.

[7] S. Chen, S. Li, Z. Ye, Y. Zhang, S. Gao, H. Rong, J. Zhang, L. Deng, A. Dong, *Chem. Eng. J.*, **2022**, 446, 136985.

[8] X. Qi, X. Tong, S. You, R. Mao, E. Cai, W. Pan, C. Zhang, R. Hu, J. Shen, *ACS Macro Lett.*, **2022**, 11, 861.

[9] W. Weng, J. Chi, Y. Yu, C. Zhang, K. Shi, Y. Zhao, *ACS Appl. Mater. Interfaces*, **2021**, 13, 4564.

[10] Y. Wang, H. Lu, M. Guo, J. Chu, B. Gao, B. He, *Adv. Healthc. Mater.*, **2021**, 11,

2101659.

[11] Y. Zhang, D. Wang, M. Gao, B. Xu, J. Zhu, W. Yu, D. Liu, G. Jiang, *ACS Biomater. Sci. Eng.*, **2018**, 4, 2879.

[12] X. Luo, Q. Yu, Y. Liu, W. Gai, L. Ye, L. Yang, Y. Cui, *ACS Sens.*, **2022**, 7, 1347.

[13] J. Chi, X. Zhang, C. Chen, C. Shao, Y. Zhao, Y. Wang, *Bioact. Mater.*, **2020**, 5, 253.

[14] W. Chen, J. Wainer, S. W. Ryoo, X. Qi, R. Chang, J. Li, *Sci. Adv.*, **2022**, 8, eabk1792.

[15] Y. Zhu, S. Li, Y. Li, H. Tan, Y. Zhao, L. Sun, *Chem. Eng. J.*, **2022**, 449, 137786.

[16] H. Jeong, J. Bae, J. Park, S. Baek, G. Kim, M. Park, J. Park, *J. Control. Release*, **2020**, 324, 280.

[17] Z. Guo, H., Z. Shi, L. Lin, Y. Li, M. Wang, G. Pan, Y. Lei, L. Xue, *J. Mat. Chem. B*, **2022**, 10, 3501.

[18] J. Chi, L. Sun, L. Cai, L., C. Shao, L. Shang, Y. Zhao, *Bioact. Mater.*, **2021**, 6,3507.

[19] S. Yao, J. Chi, Y. Wang, Y. Zhao, Y. Luo, Y. Wang, *Adv. Healthc. Mater.*, **2021**, 10, 2100056.

[20] Z. Zeng, G. Jiang, Y. Sun, U. E. Aharodnikau, K. E. Yunusov, X. Gao, T. Liu, S. O. Solomevich, *Biomater. Sci.*, **2022**, 10, 5326.

[21] M. Yin, J. Wu, M. Deng, P. Wang, G. Ji, M. Wang, C. Zhou, N. T. Blum, W. Zhang, H. Shi, N. Jia, X. Wang, P. Huang, *ACS Nano*, **2021**, 15, 17842.

[22] T. Liu, G. Jiang, G. Song, Y. Sun, X. Zhang, Z. Zeng, *J. Pharm. Sci.*, **2021**, 110,

3004.

[23] X. Zhang, G. Chen, L. Sun, F. Ye, X. Shen., Y. Zhao, *Chem. Eng. J.*, **2021**, 406, 126741.

[24] D. Han, R. S. Morde, S. Mariani, A. A. L. MAattina, E. Vignali, C. Yang, G. Barillaro, H. Lee, *Adv. Funct. Mater.*, **2020**, 30, 1909197.

[25] L. Shi, X. Liu, W. Wang, L. Jiang, S. Wang, *Adv. Mater.*, **2018**, 31, 1804187.

[26] X. Zhang, G. Chen, L. Cai, Y. Wang, L. Sun, Y. Zhao, *Chem. Eng. J.*, **2021**, 414, 128905.

[27] X. Fu, X. Zhang, D. Huang, L. Mao, Y. Qiu, Y. Zhao, *Chem. Eng. J.*, **2022**, 431,133362.

[28] J. Chi, X. Zhang, C. Chen, C. Shao, Y. Zhao, Y. Wang, *Bioact. Mater.*, **2020**, 5, 253.

[29] N. Bandara, J. Wu, *ACS Sustain. Chem. Eng.*, **2018**, 6,1152.

[30] J. Yang, H. Yu, L. Wang, J. Lium X. Liu, Y. Hong, Y. Huang, S. Ren, *Eur. Polym. J.*, **2022**, 172,111241.

[31] B. Ciui, A. Martin, R. K. Mishra, B. Brunetti, T. Nakagawa, T. J. Dawkins, M. Lyu, C. Cristea, R. Sandulescu, J. Wang, *Adv. Healthc. Mater.*, **2018**, 7,1701264.

[32] X. Zhang, G. Chen, Y. Yu, L. Sun, Y. Zhao, *Research*, **2022**, 2020, 3672120.

[33] Z. Chen, Y. Lin, W. Lee, L. Ren, B. Liu, L. Liang, Z. Wang, L. Jiang, *ACS Appl. Mater. Interfaces*, **2018**,10, 29338.

[34] A. C. Noel, D. L. Hu, *Proc. Natl. Acad. Sci. U. S. A.*, **2018**, 115, 12377.

[35] W. K. Cho, J. A. Ankrum, D. Guo, J. M. Karp, *Proc. Natl. Acad. Sci. U. S. A.*, **2012**, 109, 21289.

[36] M. Yin, J. Wu, M. Deng, P. Wang, G. Ji, M. Wang, C. Zhou, N. T. Blum, W. Zhang, H. Shi, N. Jia, X. Wang, P. Huang, *ACS Nano*, **2021**, 15, 17842.

[37] R. Yu, H. Zhang, B. Guo, *Nano-Micro Lett.*, **2022**, 14, 1.

[38] J. I., K. MinPark, K. D. Park, *J. Ind. Eng. Chem.*, **2019**, 69, 397.

[39] L. Ruan, G. Song, X. Zhang, T. Liu, Y. Sun, J. Zhu, Z. Zeng, G. Jiang, *Biomater. Sci.*, **2021**, 9, 6830.

[40] M. Zhang, R. Song, Y. Liu, Z. Yi, X. Meng, J. Zhang, Z. Tang, Z. Yao, Y. Liu, X. Liu, W. Bu, *Chem*, **2019**, 5, 2171.

[41] B. Liu, S. Liang, Z. Wang, Q. Sun, F. He, S. Gai, P. Yang, Z. Cheng, J. Lin, *Adv. Mater.*, **2021**, 33, 3101223.

[42] H. Kim, J. Kim, J. Park, K. Baek, *J. Hazard. Mater.*, **2022**, 432, 128751.

[43] Y. Xi, J. Ge, M. Wang, M. Chen, W. Niu, W. Cheng, Y. Xue, C. Lin, B. Lei, *ACS Nano*, **2020**, 14, 2904.

[44] W. Li, X. Jian, Y. Zou, L. Wu, H. Huang, H. Li, D. Hu, B. Yu, *Front. Bioeng. Biotechnol.*, **2021**, 9, 709679.

[45] Z. Guo, Z. Zhang, N. Zhang, W. Gao, J. Li, Y. Pu, B. He, J. Xie, *Bioact. Mater.*,

2022, 15, 203.

[46] M. Guo, Y. Wang, B. Gao, B. He, *ACS Nano*, **2021**, 15, 15316.

[47] L. Jin, X. Guo, D. Gao, Y. Liu, J. Ni, Z. Zhang, Y. Huang, G. Xu, Z. Yang, X. Zhang, X. Jiang, *Bioact. Mater.*, **2022**, 16, 162.

[48] S. Yu, G. Li, P. Zhao, Q. Cheng, Q. He, D. Ma, W. Xue, *Adv. Funct. Mater.*, **2019**, 29, 1905697.

[49] M. Cieślak, D. Kowalczyk, M. Krzyżowska, M. Janicka, E. Witczak, I. Kamińska, *Materials*, **2022**, 15, 6164.

[50] C. Hu, L. Long, J. Cao, S. Zhang, Y. Wang, *Chem. Eng. J.*, **2021**, 411, 128564.

[51] X. Zhao, Y. Liang, Y. Huang, J. He, Y. Han, B. Guo, *Adv. Funct. Mater.*, **2020**, 30, 1910748.

[52] X. Shi, Z. Chen, Y. He, Q. Lu, R. Chen, C. Zhao, D. Dong, Y. Sun, H. He, *Carbohydr. Polym.*, **2022**, 297, 120042.

[53] C. Tong, X. Zhong, Y. Yang, X. Liu, G. Zhong, C. Xiao, B. Liu, W. Wang, X. Yang, *Biomaterials*, **2020**, 243, 119936.

[54] Q. Xu, M. Chang, Y. Zhang, E. Wang, M. Xing, L. Gao, Z. Huan, F. Guo, J. Chang, *ACS Appl. Mater. Interfaces*, **2020**, 12, 31255.

[55] J. Xiao, Y. Zhu, S. Huddleston, P. Li, B. Xiao, O. K. Farha, G. A. Ameer, *ACS Nano*, **2018**, 12, 1023.

[56] R. Li, Z. Cheng, R. Wen, X. Zhao, X. Yu, L. Sun, Y. Zhang, Z. Han, Y. Yuan, L. Kang, *RSC Adv.*, **2018**, 8, 15558.

[57] Y. Lu, H. Li, J. Wang, M. Yao, Y. Peng, T. Liu, Z. Li, G. Luo, J. Deng, *Adv. Funct. Mater.*, **2021**, 31, 215749.

[58] Z. Guo, H. Liu, Z. Shi, L. Lin, Y. Li, M. Wang, G. Pan, Y. Lei, L. Xue, *J. Mat. Chem. B*, **2022**, 10, 3501.

[59] P. Li, L. Ruan, G. Jiang, Y. Sun, R. Wang, X. Gao, K. E. Yunusov, U. E. Aharodnikau, S. O. Solomevich, *Acta Biomater.*, **2022**, doi, 10.1016/j.actbio.2022.08.075.

[60] Z. Xu, G. Liu, P. Liu, Y. Hu, Y. Chen, Y. Fang, G. Sun, H. Huang, J. Wu, *Acta Biomater.*, **2022**, 147, 147.

[61] B. Z. Johnson, A. W. Stevenson, C. M. Prele, M. W. Fear, F. M. Wood, *Biomedicines*, **2020**, 8, 101.